JACS
JOURNAL OF THE AMERICAN CHEMICAL SOCIETY
pubs.acs.org/JACS
Article

Crystalline C—C and C═C Bond-Linked Chiral Covalent Organic Frameworks

Chen Yuan, Shiguo Fu, Kuiwei Yang, Bang Hou, Yan Liu,* Jianwen Jiang, and Yong Cui*

Cite This: https://dx.doi.org/10.1021/jacs.0c11050

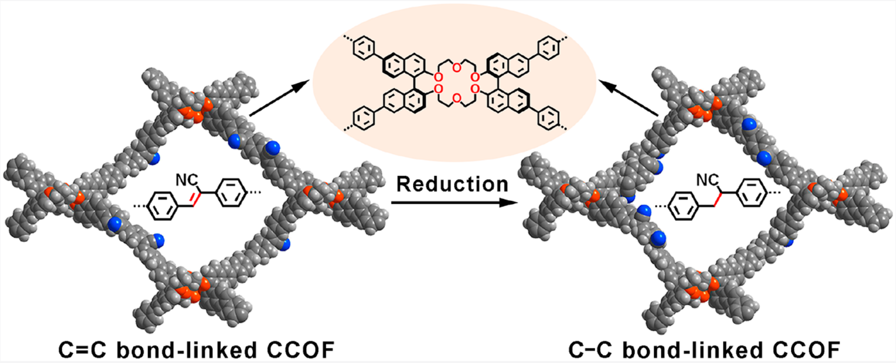

ABSTRACT: While crystalline covalent organic frameworks (COFs) linked by C−C bonds are highly desired in synthetic chemistry, it remains a formidable challenge to synthesize. Efforts to generate C−C single bonds in COFs via de novo synthesis usually afford amorphous structures rather than crystalline phases. We demonstrate here that C−C single bond-based COFs can be prepared by direct reduction of C═C bond-linked frameworks via crystal-to-crystal transformation. By Knoevenagel polycondensation of chiral tetrabenzaldehyde of dibinaphthyl-22-crown-6 with 1,4-phenylenediacetonitrile or 4,4′-biphenyldiacetonitrile, two olefin-linked chiral COFs with 2D layered tetragonal structure are prepared. Reduction of olefin linkages of the as-prepared CCOFs produces two C−C single bond linked frameworks, which retains high crystallinity and porosity as well as high chemical stability in both strong acids and bases. The quantitative reduction is confirmed by Fourier transform infrared and cross-polarization magic angle spinning ^{13}C NMR spectroscopy. Compared to the pristine structures, the reduced CCOFs display blue-shifted emission with enhanced quantum yields and fluorescence lifetimes, while the parent CCOFs exhibit higher enantioselectivity than the reduced analogs when be used as fluorescent sensors to detect chiral amino alcohols via supramolecular interactions with the built-in crown ether moieties. This work provides an attractive strategy for making chemically stable functionalized COFs with new linkages that are otherwise hard to produce.

■ INTRODUCTION

Covalent organic frameworks (COFs), an attractive class of porous crystalline polymers,[1] have been widely explored for applications in diverse areas such as storage,[2] separation,[3] and catalysis[4] because of their tunable structures and chemical properties. The crystallinity, stability, and functions of COFs are dictated by the type of covalent linkages that join the molecular building blocks. By far, covalent linkages varying from reversible boroxine, imine, and hydrazone; less reversible triazine, phenazine, and oxazole; to almost nonreversible dioxin and olefin have been reported to construct COFs.[5] It is believed that making C−C single bond-linked COFs would address the chemical stability issues of the network linkages while also producing materials with new properties. However, efforts to produce C−C single bonds in COFs via de novo synthesis typically afford amorphous structures rather than crystalline phases.[6] On the other hand, despite their potential use in enantioselective catalysis, separation, and sensing,[7] the synthesis of chiral COFs (CCOFs) linked by less reversible bonds has not yet be explored.[8] In this work, we illustrated that C−C single bond linked CCOFs can be synthesized by reduction of olefin-linked frameworks via crystal-to-crystal transformation. Interestingly, postsynthetic methods have recently been explored to convert imine linkages in COFs to other linkages such as amide and amine.[9]

Macrocyclic compounds such as crown ethers have been the focus of intense research interest for decades because of their superior selectivity in complexation with metal ions and

Received: October 20, 2020

Scheme 1. Synthesis of the COFs

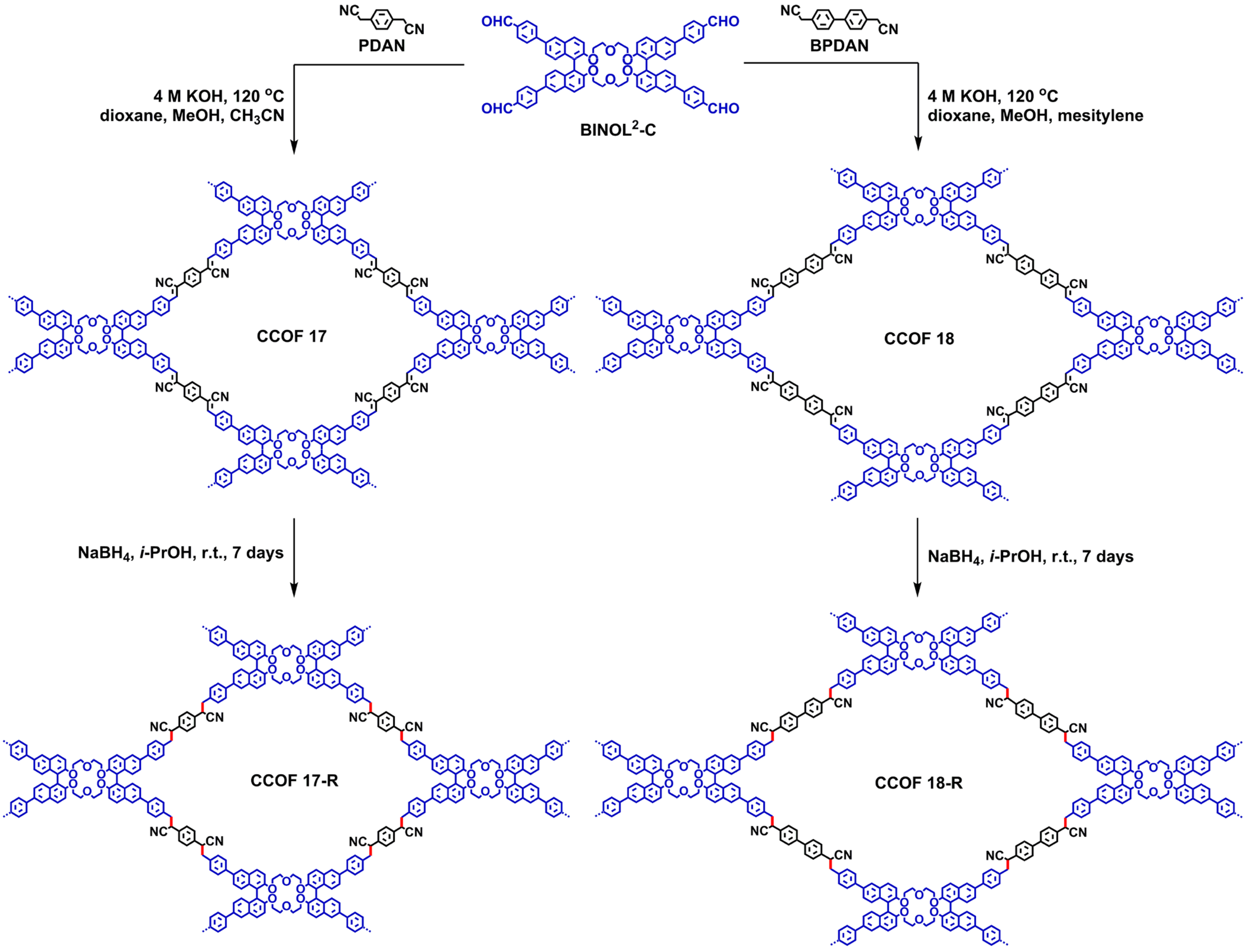

organic cations.[10] Chiral crown ethers are capable of binding protonated chiral primary amines with high stereoselectivity and affinity and have been extensively employed to resolve or distinguish the enantiomers of chiral amines. However, chiral crown ethers have not yet been used in construction of CCOFs for enantioselective processes, in spite of several related metal−organic frameworks (MOFs) having been reported.[11] Herein, an enantiopure tetrabenzaldehyde derived from dibinaphthyl-22-crown-6 (**BINOL^2-C**, Scheme 1), which has as the dialdehyde primary functionality and 22-crown-6 secondary functionality, was designed and synthesize to crystallize CCOFs. It is worth noting that, owing to its axial chirality characteristic, optically active 1,1′-bi-2-naphthol (BINOL) has become a key source of chirality for organic synthesis and materials science and provides an attractive platform for asymmetric catalysis and enantioselective recognitions.[12] By Knoevenagel polycondensation of **BINOL^2-C** with 2,2′-(1,4-phenylene)diacetonitrile (**PDAN**) or 2,2′-(biphenyl-4,4′-diyl) diacetonitrile (**BPDAN**), the first two examples of olefin-linked CCOFs that have a 2D layered tetragonal structure were prepared. Reduction of olefin linkages of the as-prepared frameworks produces the first two examples of C−C single bond-linked CCOFs, which retains crystallinity and porosity as well as chemical stability (Scheme 1). Compared to the parent CCOFs, the reduced frameworks display blue-shifted emission with enhanced quantum yields and fluorescence lifetimes; whereas the parent CCOFs exhibit better enantioselectivity than the reduced materials when used as fluorescent sensors to detect amino alcohols via supramolecular interactions with the immobilized crown ether moieties.

RESULTS AND DISCUSSION

Synthesis and Characterization. CCOFs **17** and **18.** The enantiopure monomer **BINOL^2-C** was prepared by Suzuki coupling reaction between bromobenzene derivate of dibinaphthyl-22-crown-6 and 4-formylphenylboronic acid. CCOFs **17** and **18** were then prepared by solvothermal reactions of **BINOL^2-C** (0.064 mmol), 2,2′-(1,4-phenylene) diacetonitrile (**PDAN**; 0.128 mmol) or 2,2′-(biphenyl-4,4′-diyl)-diacetonitrile (**BPDAN**; 0.128 mmol) in dioxane (0.5 mL), methanol (0.5 mL) and acetonitrile (0.2 mL) or mesitylene (0.1 mL) in the presence of KOH solution as a catalyst at 120 °C. After 4 days, the reactions afforded bright yellow microcrystalline solids in about 85% yields. Notably, although K$^+$ and crown ethers tend to form stable host−guest adducts, inductively coupled plasma optical emission spectrometer (ICP-OES) of the digested crystals showed the contents of potassium are only 0.009% and 0.021% for CCOFs **17** and **18**, respectively.

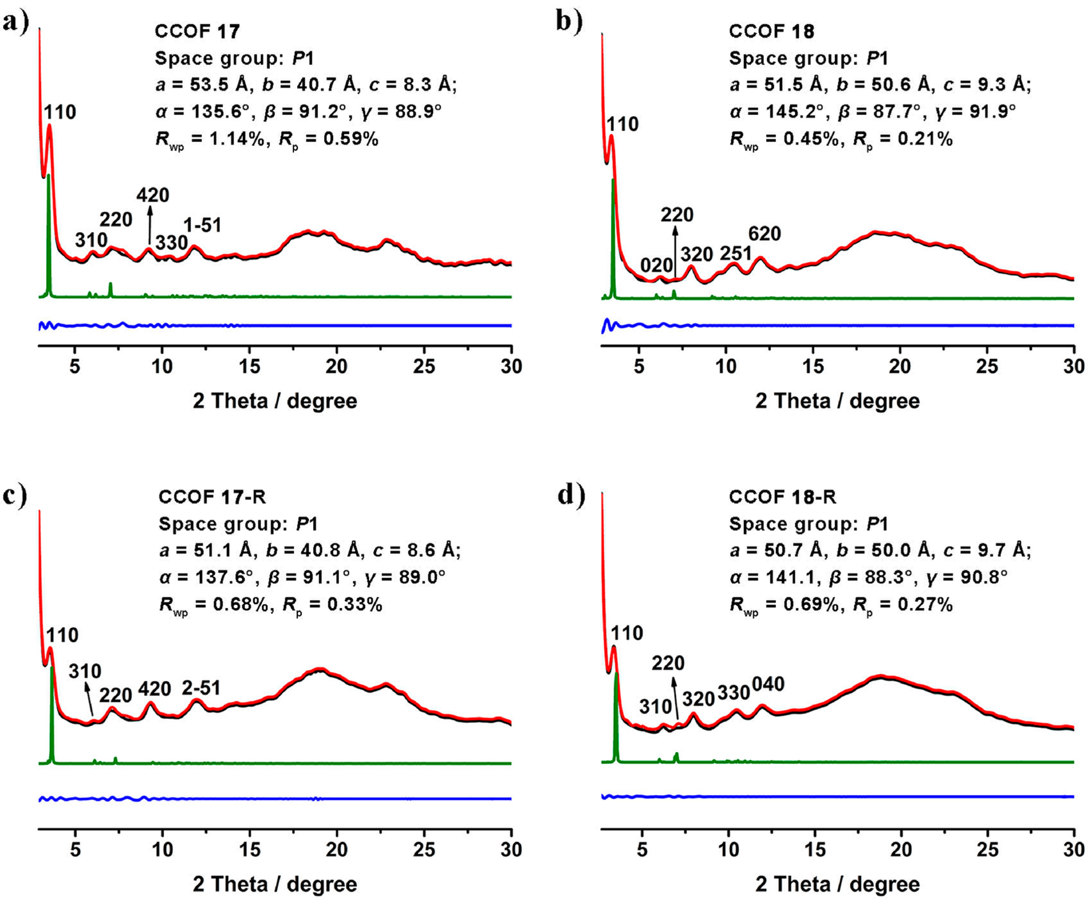

Figure 1. (a−d) PXRD patterns of the four CCOFs with the experimental profiles in red, Pawley refined in black, calculated in dark green, and the difference between the experimental and refined PXRD patterns in blue.

The as-prepared COFs were characterized by a variety of spectroscopic techniques. The Fourier transform infrared (FT-IR) spectra of the two sp^2-carbon-linked conjugated CCOFs (sp^2c-CCOFs) show a great decrease of the characteristic C═O vibration band (1690 cm^{-1}) and the newly appearance of the C≡N vibration band (1620 cm^{-1}), indicating the successful polymerization (Figure S1). The ^{13}C cross-polarization magic angle spinning (CP-MAS) NMR spectra show that the aldehyde carbon peaks were barely observed and the C═C linkages were observed at ∼110 and ∼190 ppm (Figure 3b,c). The chemical shifts of other fragments are in good agreement with those of the monomers. Thermal gravimetric analysis (TGA) reveals that both sp^2c-CCOFs are stable up to 350 °C (Figure S2). Scanning electron microscopy (SEM) and transmission electron microscopy (TEM) images show that both of them possess uniform layered morphology (Figures 3d and S3). Circular dichroism (CD) spectra of these sp^2c-CCOFs made from (*R,R*)- and (*S,S*)-enantiomers of the dibinaphthyl-22-crown-6 monomers are mirror images of each other, which is indicative of their enantiomeric nature (Figure S4).

Crystal Structure. The crystalline structures of the CCOFs were determined by powder X-ray diffraction (PXRD) analysis with Cu Kα radiation (Figure 1). Considering the geometry of the precursors and the connection patterns, a few 2D and 3D topologies are reasonable. However, considering their layered morphology observed by SEM and TEM, 2D topologies are more rational. After a geometrical energy minimization based on the 2D net with AA stacking mode for CCOF **17**, the unit cell parameters were obtained (a = 53.5 Å, b = 40.7 Å, c = 8.3 Å, α = 135.6°, β = 91.2°, and γ = 88.9°). The experimental PXRD pattern for CCOF **17** with *P*1 space group exhibited main diffraction peaks at 3.55°, 6.02°, 7.13°, 9.21°, 10.46°, and 11.85°, which were assigned to the (110), (310), (220), (420), (330), and (1−51) facets, respectively. This PXRD pattern was in good agreement with the simulated pattern based on AA stacking structure of CCOF **17**, suggesting that the material holds a single-pore structure. The lattice modeling and Pawley refinement (Materials Studio, version 7.0) provide good agreement factors (R_p = 0.59% and R_{wp} = 1.14%).

The experimental PXRD pattern for CCOF **18** with a *P*1 space group exhibited main peaks at 3.36°, 6.61°, 7.03°, 7.97°, 10.44°, and 11.92°, which were assigned to the (110), (020), (220), (320), (251), and (620) facets, respectively. This PXRD pattern agreed well with the simulated pattern based on the AA stacking structure. The refinement results yield unit cell parameters are nearly equivalent to the predictions that a = 51.5 Å, b = 50.6 Å, c = 9.3 Å, α = 145.2°, β = 87.7°, and γ = 91.9° (R_p = 0.21% and R_{wp} = 0.45%). PXRD patterns were also calculated for the two CCOFs on the other 2D and 3D structures, but all of the calculated PXRD patterns did not match the experimental patterns well (Figures S5−S12). CCOFs **17** and **18** are therefore proposed to have a slipped AA stacking structure (Figure 2).

We failed to calculate the pore size distributions of these two sp^2c-CCOFs by measuring nitrogen sorption isotherms because of the low adsorption of N_2. This is probably due to the distortion of frameworks containing flexible crown ether

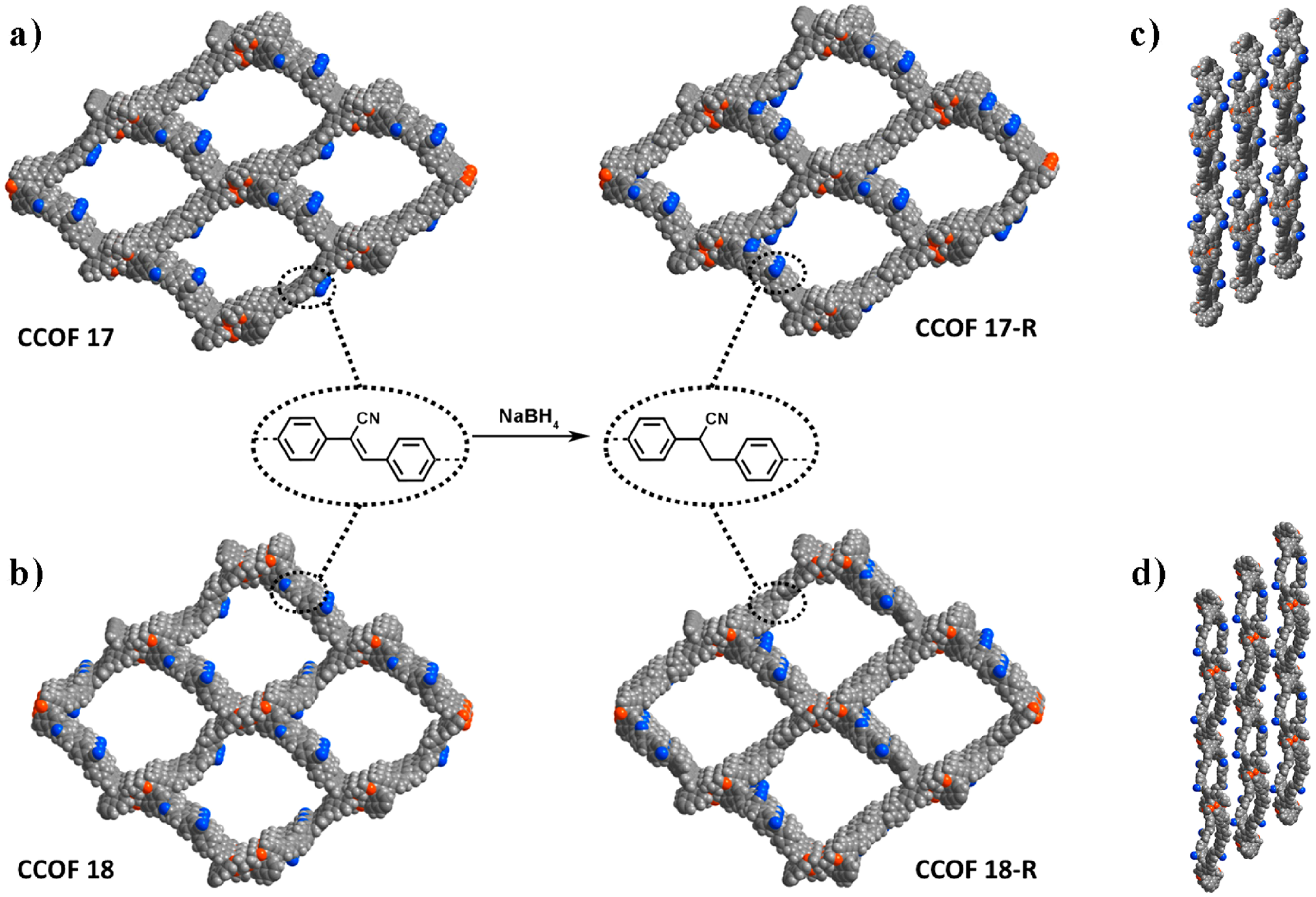

Figure 2. Top views of the corresponding refined structure of (a) CCOF **17** (left) and CCOF **17**-R (right) and (b) CCOF **18** (left) and CCOF **18**-R (right). Side views of the slipped AA stacking structure of (c) CCOF **17** and (d) CCOF **18**. Carbon, gray; nitrogen, blue; oxygen, red; hydrogen, light gray.

moieties upon solvent removal.[13a] So, we used a dye uptake assay to evaluate the pore size distribution of the CCOFs.[9b,13] We carried out dye-uptake studies by soaking the COFs in a solution of dyes with different sizes for 24 h. The dye solution was decanted, and the COFs were washed several times to remove dye molecules adsorbed on the external surfaces of the solids. Dye molecules and COFs after spectral separation can be assigned to red and green fluorescence by confocal fluorescence microscopy (CFM), respectively (Figures 4b and S13). The CFM results showed the uniform distributions of dyes **A**−**C** with molecular sizes ranging from 1.40 × 1.60 nm^2 to 2.20 × 2.40 nm^2. However, the sterically bulky dye **D** (3.20 × 3.60 nm^2) was only attached to the surfaces of the COFs and cannot enter the pores from the open channels, probably due to its larger size. The dye absorption amount was determined by measuring the UV−vis spectra in THF (Figures S14 and S15). As shown in Figure 4c, remarkable size selectivity was observed for the dye uptake: the COFs had very significant uptake of dyes **A**−**C** (1.4−7.9 wt%) but had only negligible uptake of dye **D** (<0.3 wt%). The dye uptake experiment indicated that both the maximum pore diameter and opening of the two COFs were in the range of 2.4 to 3.2 nm, consistent with the crystal structures.

CCOFs 17-R and 18-R. Both of them were prepared by direct reduction of the olefin-linked CCOFs via crystal-to-crystal transformation. In order to identify a suitable condition to realize solid-state conversion of C$=$C linkages to C−C bonds in CCOFs, we selected a commercially available compound, 2,3-diphenylacrylonitrile (DPAN), as a model molecule. Among various reductive conditions tested, we identified that the best method involving the use of NaBH$_4$, by which quantitative conversion of DPAN to 2,3-diphenylpropionohnitrile (DPPN) was realized (Figure 3a). This was confirmed by the shift of C$\equiv$N vibration peaks from 2218 to 2241 cm^{-1} in the FT-IR spectrum of the product. ^{13}C NMR spectra of the model compounds are another evidence for the reduction of C$=$C bond. The peaks belong to sp^2-carbon at 126 and 143 ppm disappeared completely and new peaks at 40 and 42 ppm emerged, indicating the formation of C−C bond.

The mixture of CCOF **17** or **18** (10 mg), NaBH$_4$ (100 mg), and 2 mL of *i*-PrOH stood at r.t. for 3 days, then another part of NaBH$_4$ (100 mg) was added, and the mixture stood for another 4 days to achieve the successfully conversion of olefin CCOFs to C−C bond linked **17**-R and **18**-R (see the Supporting Information for details). The quantitative reduction was confirmed by the appearance of a new peak at 2241 cm^{-1} from the C$\equiv$N vibration band in the FT-IR spectrum of both CCOFs **17**-R and **18**-R (Figure 4b,c). Besides, the ^{13}C CP-MAS NMR spectra showed peaks shifts due to the formation of a C−C bond. Peaks that belong to sp^2 carbon at 103 and 189 ppm disappeared completely, and new peaks at 35 and 60 ppm emerged for CCOF **17**-R. For CCOF **18**-R, peaks that belong to sp^2 carbon at 111 and 189 ppm disappeared

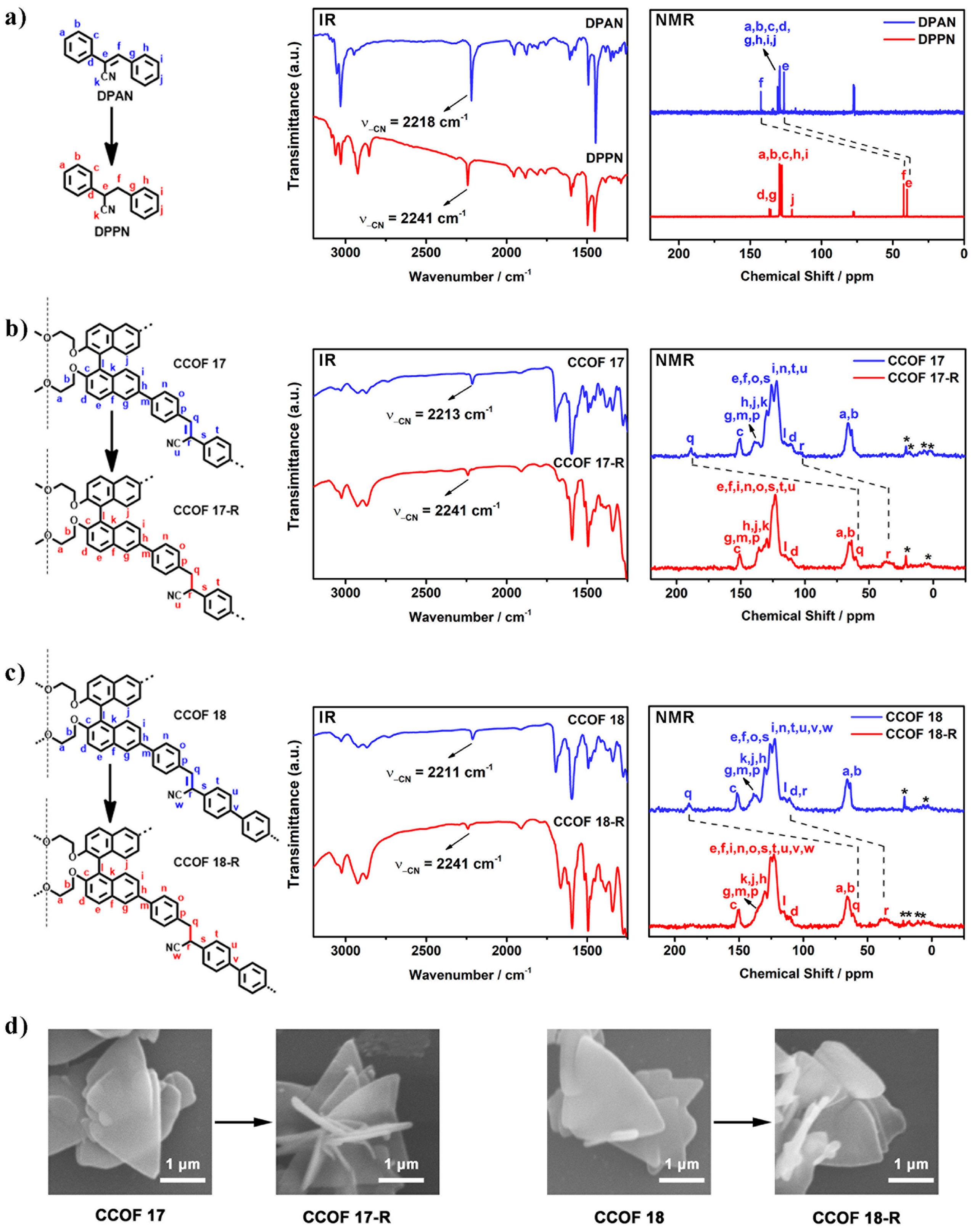

Figure 3. Scheme for reduction of (a) the model molecule, (b) CCOF **17**, and (c) CCOF **18**. Corresponding FTIR spectra and ^{13}C NMR spectra are in the right. *, sidebands. (d) SEM images of the parent and reduced CCOFs.

when new peaks at 36 and 61 ppm emerged, indicating the successful reduction of CCOF **18**.

PXRD patterns of the reduced CCOFs are almost the same with the pristine CCOFs, although decreases in signal-to-noise ratio of the peaks were observed, verifying that the crystalline structures of COFs were retained after reduction (Figure 1c,d). The additional flexibility of C−C bond linkages compared to C═C bond linkages prevents tight stacking between layers

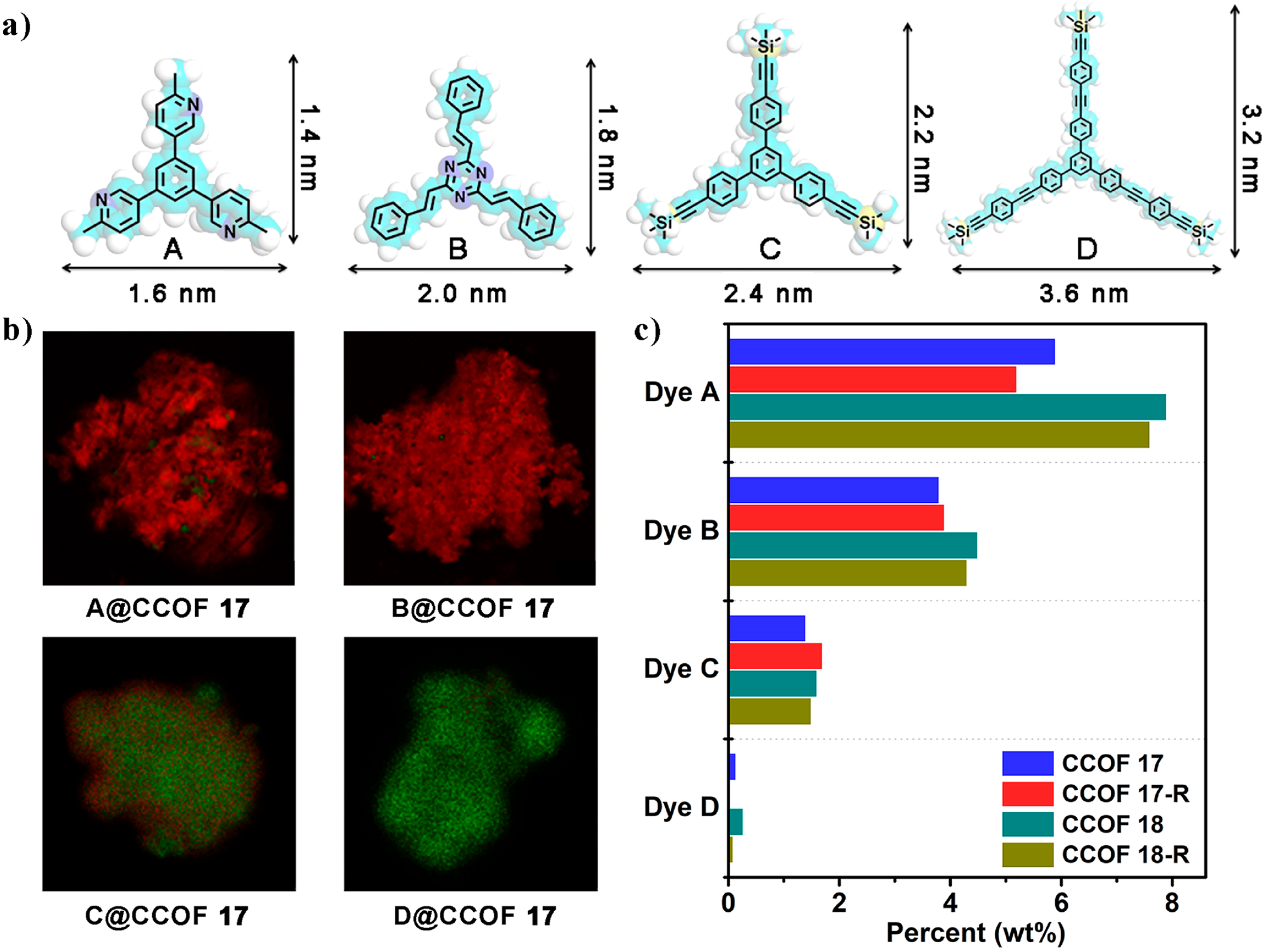

Figure 4. (a) Structure and molecular sizes of dyes **A**–**D**. (b) CFM images obtained from CCOF **17** after incubation with dyes **A**–**D**, respectively. (c) Different dye uptake of CCOFs by UV–vis spectroscopy.

and leads to slightly decreased crystalline. When finishing the geometrical energy minimization based on the 2D net mode, the unit cell parameters of CCOF **17**-R were obtained (a = 51.1 Å, b = 40.8 Å, c = 8.6 Å, α = 137.6°, β = 91.1°, and γ = 89.0°). The experimental PXRD pattern for CCOF **17** with $P1$ space group exhibited main diffraction peaks at 3.55°, 6.08°, 7.15°, 9.32°, and 11.96°, which were assigned to the (110), (310), (220), (420), and (2−51) facets, respectively. This PXRD pattern was in good agreement with the simulated pattern based on AA stacking structure of CCOF **17**-R. The lattice modeling and Pawley refinement provide good agreement factors (R_p = 0.33% and R_{wp} = 0.68%). For CCOF **18**-R, the experimental PXRD pattern with $P1$ space group exhibited peaks at 3.36°, 6.23°, 7.07°, 7.97°, 10.48°, and 11.94°, which were assigned to the (110), (310), (220), (320), (330), and (040) facets, respectively. This PXRD pattern also agreed well with the simulated pattern based on the AA stacking structure of CCOF **18**-R. The refinement results yield unit cell parameters that are nearly equivalent to the predictions that a = 50.7 Å, b = 50.0 Å, c = 9.7 Å, α = 144.1°, β = 88.3°, and γ = 90.8° (R_p = 0.27% and R_{wp} = 0.69%). So, CCOFs **17**-R and **18**-R are proposed to have the architectures as illustrated in Figure 2.

Dye uptake experiments and the CFM results revealed that the maximum pore diameter of CCOFs **17**-R and **18**-R were in the range of 2.4 to 3.2 nm, indicating retention of porous structures of the parent frameworks (Figures 4c and S13–S15). SEM and TEM images showed that both reduced frameworks had a uniform layered morphology (Figures 3d and S3), indicating that the crystal morphology remained unchanged after the solid-state conversion. In TGA curves of CCOF **17**-R and **18**-R, the weight loss was also observed in the temperature above 350 °C (Figure S2), which is almost the same as the parent CCOFs.

Chemical Stability. To evaluate the chemical stability of CCOFs, we immersed them for 1 week in various solvents, including THF, DMF, MeOH, water, concentrated HCl (6 M), and aqueous KOH (14 M) solutions. From PXRD data (Figures 5a,b and S16), CCOFs **17** and **18** are stable and retained their crystallinity. Notably, **17** and **18** exhibited nearly no weight loss (<1 wt%) in common organic solvents, even under strong acidic (6 M HCl) and basic (14 M KOH) conditions; the residual weight percentages were as high as 93 and 88 wt% for **17** and 95 and 93 wt% for **18** (Figure S17). Also, we did the dye **A** uptake experiment to check the preservation of pore structure. It was found that the dye absorption amount of **17** and **18** after treating with various solvents showed almost no decrease, indicating retention of their porous structures (Figure 5c,d).

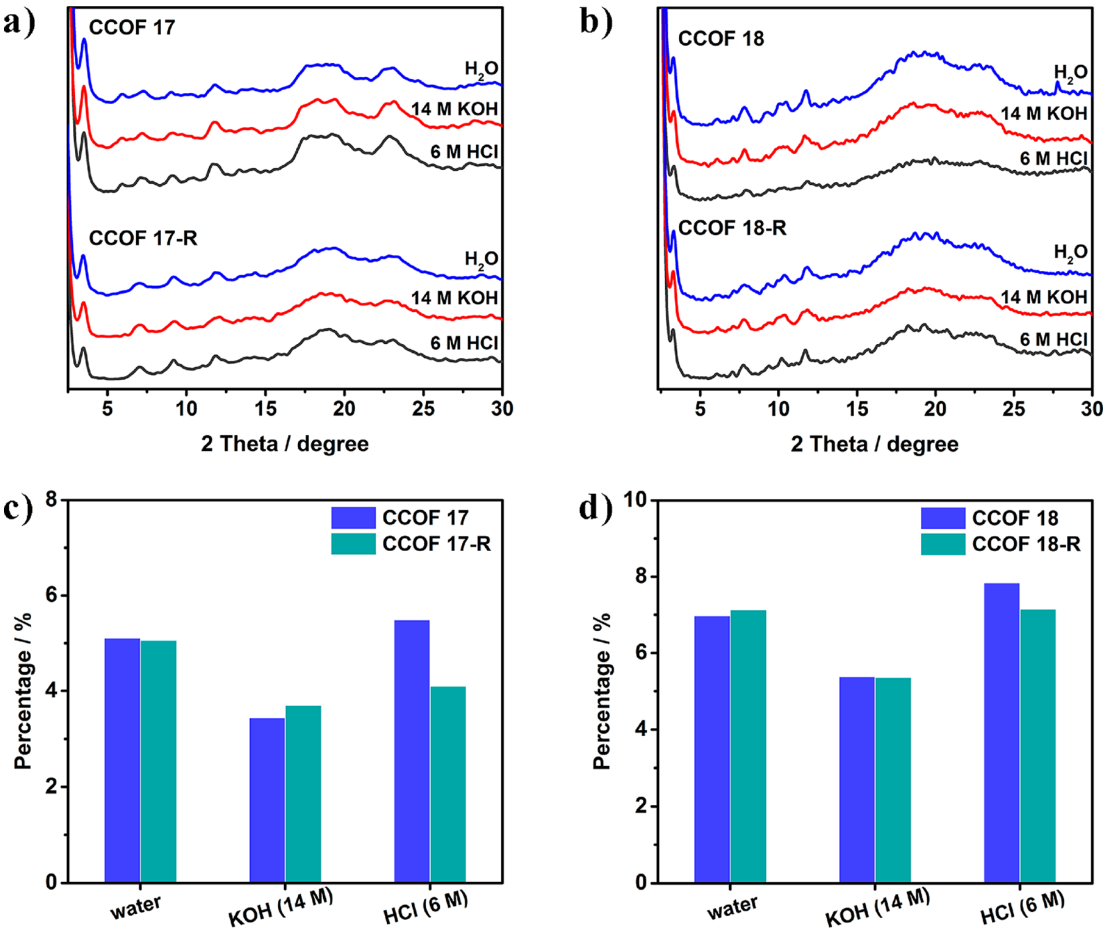

Figure 5. PXRD patterns of (a) CCOFs **17** and **17**-R and (b) CCOF **18** and **18**-R after treatment in different solvents for 1 week. Dye **A** uptake of (c) CCOFs **17** and **17**-R and (d) CCOFs **18** and **18**-R after treatment in different solvents for 1 week by UV−vis spectroscopy.

As expected, CCOFs **17**-R and **18**-R keep crystallinity and porosity after soaking in concentrated HCl (6 M) and aqueous KOH (14 M) solutions for 1 week, as indicated by PXRD (Figure 5a,b). From the residual weight percentages, they exhibit nearly no weight loss (<1 wt%) in organic solvents and little weight loss (<10 wt%) under strong acid (6 M HCl) and base (14 M KOH; Figure S17). After these treatments, CCOF **17**-R and **18**-R can uptake 3−6 and 5−8 wt% of dye **A**, respectively, which are close to those of the as-synthesized samples (Figure 5c,d). The present frameworks represent the most stable CCOFs that have been reported thus far (Figure S18).[8] Obviously, the good chemical stability of these CCOFs are attributed to the stable C═C bond and C−C bond linkages.

Enantioselective Fluorescence Recognition. The photophysical properties of CCOFs were studied by UV−vis, fluorescent and circular dichroism (CD) spectra, and compared with the homogeneous control **P-BINOL^2-C**, which was prepared by the Knoevenagel condensation of **BINOL^2-C** and phenylacetonitrile (for details see section 2.3 in the Supporting Information).

As shown in Figure 6, CCOFs **17**, **17**-R, **18**, and **18**-R absorb light in the UV and visible regions, with absorption maxima at 422, 396, 422, and 397 nm, respectively, which are red-shifted by 5−40 nm in comparison to that of the **BINOL^2-C** monomer, due to the conjugation in the crystalline structures. Upon illumination with UV light, CCOFs **17** and **18** gave emission maxima at 527 and 511 nm with quantum yields (ϕ_{PL}) of 5.8% and 6.5%, respectively (Figure 6 and Table S1), different from **P-BINOL^2-C**, which emitted around 495 nm with ϕ_{PL} of 17.5%. Time-resolved fluorescence spectroscopy revealed that **17** and **18** have a lifetime (τ) of 0.83 and 0.88 ns, which is smaller than 1.65 ns of **P-BINOL^2-C** (Table S1). The decreased ϕ_{PL} and τ values suggest that the $\pi-\pi$ interactions between layers of sp^{2}c-CCOFs facilitate the nonradiation energy transfer. Interestingly, after reduction, the emission maxima of **17**-R and **18**-R were blue-shifted to 507 and 493 nm with ϕ_{PL} of 19.0% and 20.5% and τ of 2.10 and 2.04 ns, respectively. Compared to the parent CCOFs, the reduced CCOFs show increased ϕ_{PL} and τ values. It is likely that the newly formed C−C bond linkages destroyed the π-conjugated structure of sp^{2}c-CCOFs, leading to the decrease of $\pi-\pi$ interactions between COF layers and limiting the nonradiation energy transfer.[14] In addition, CD spectra of CCOFs made from the opposite enantiomers were mirror images of each other, suggesting their enantiomeric nature (Figure S4), consistent with their UV−vis spectra (Figure 6a,b).

Chiral discrimination of compounds with amino and hydroxyl functionalities is of critical importance in many areas of analytical chemistry and biotechnology.[15] The presence of chiral functional crown ether groups in these fluorescent CCOFs makes them good candidates for enantioselective recognition of chiral molecules. Crown ethers have a unique architectural feature that allows them to form various complexes with organic ammonium ions.[16] Primary

https://dx.doi.org/10.1021/jacs.0c11050
J. Am. Chem. Soc. XXXX, XXX, XXX−XXX

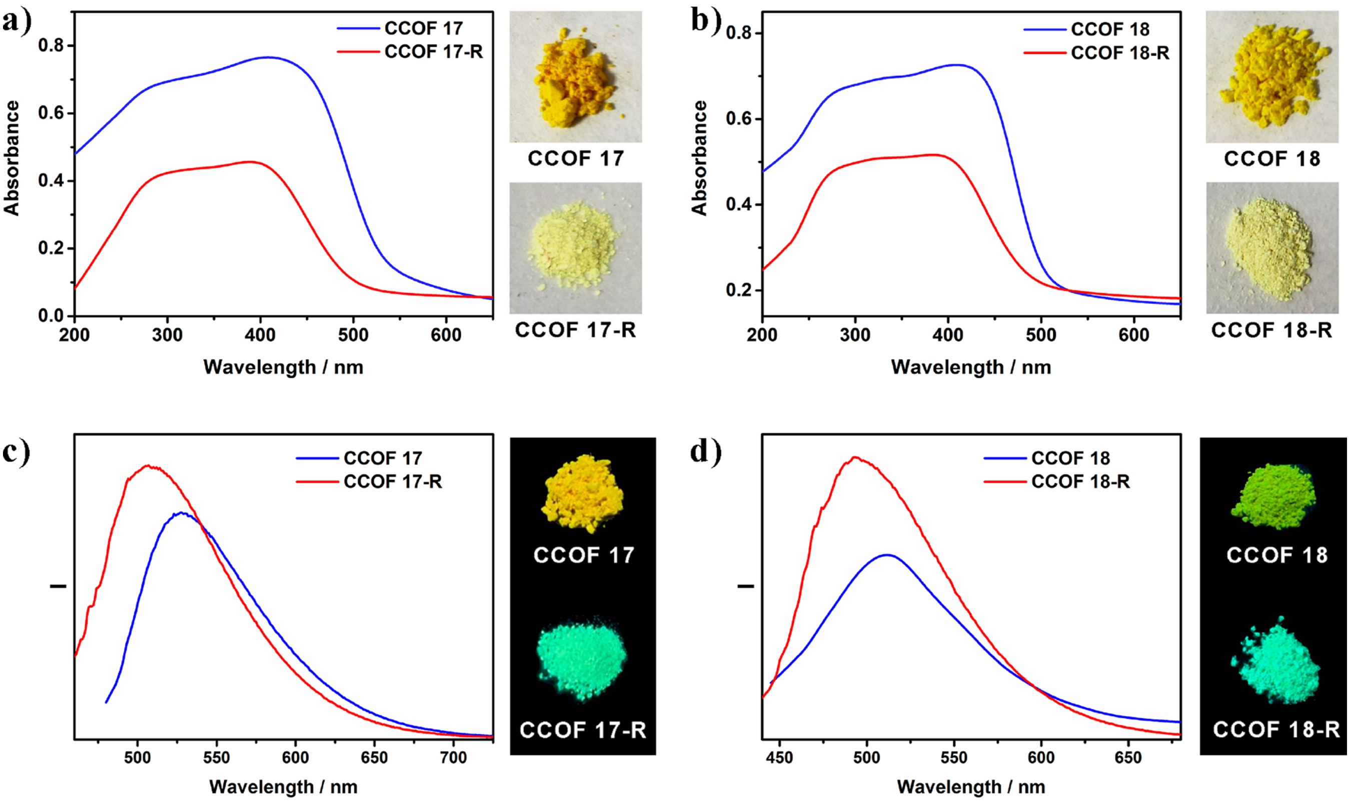

Figure 6. (a,b) Solid-state UV−vis spectra of CCOFs. Corresponding photographs of the parent and reduced CCOFs are in the right. (c,d) The solid-state fluorescence spectra of CCOFs. Corresponding photographs of the parent and reduced CCOFs under 365 nm UV light are in the right.

ammonium guests can bind to crown ethers via hydrogen bonds between their N^+−H bonds and the free electron pair atoms in crown ethers (Figure 7a). As a result, CCOFs were tested for fluorescence enhancement or quenching by amino alcohols.

Microcrystalline particles of the (*R*)-CCOFs with an average size of 1.4−2.9 μm were prepared by vigorous stirring with a magnetic stir bar and then suspended in MeOH to prepare a stock suspension with the CCOF concentration of 1×10^{-5} mol/L. The suspension was acidified by an aqueous $HClO_4$ solution (pH 1). Aliquots containing different amounts of D- and L-amino alcohol were added to the acidic MeOH suspensions of (*R*)-CCOFs (3 mL). The fluorescence emission signals of the CCOF suspension in the presence of different amounts of amino alcohols were measured. As shown in Figure 7c, when CCOF **17** was treated with phenylglycinol (PGL), the emission at 529 nm was enhanced obviously by D enantiomers, while the intensity was almost no change with L-enantiomer, indicative of enantioselectivity. The fluorescence intensity was increased to 1.36 and 1.02 times that of the original value by D- and L-phenylglycinol, respectively. The corresponding Benesi−Hildebrand plots were shown in Figure 7d. The association constants K_{BH} of **17** were calculated to be 2338.60 ± 149.38 and 158.88 ± 10.41 M^{-1} with L- and D-phenylglycinol, respectively, affording an enantioselectivity factor [EF = $K_{BH(L\text{-phenylglycinol})}/K_{BH(D\text{-phenylglycinol})}$] of 14.72. Besides, phenylalaninol (PAL) can also selectively enhance the fluorescence of CCOF **17** (Figures 7f and S20), with the EF of 12.85.

In contrast, when treated with both D- and L-tryptophanol (TPL), the fluorescence of **17** was quenched and followed Stern−Völmer (S−V) behavior. The quenching rate caused by D-tryptophanol was faster than that by the L-enantiomer, and the fluorescence intensity was decreased to 43% and 66% of the original level, respectively. Based on the linear Stern−Völmer equation, the measured absorbance [I_0/I] varied as a function of [M] in a linear relationship (Figure S20), where I_0 is the maximum fluorescence intensity before exposure to the analyte and *I* is the maximum intensity after exposure to the analyte, indicating 1:1 stoichiometry of the interaction between the crown ether of **17** and tryptophanol. The K_{sv} constants were calculated to be 820.5 M^{-1} and 340.1 M^{-1} with the D- and L-enantiomers, respectively, affording the quenching ratio [QR = $K_{sv(D\text{-tryptophanol})}/K_{sv(L\text{-tryptophanol})}$] of 2.41.

Figure 7e depicts the effect of the pH value of $HClO_4$ aqueous solution on fluorescence intensity. $HClO_4$ aqueous solutions in different pH value were added to the suspension of CCOF **17**, and the fluorescence intensity enhancement after treated with 0.083 μM D-phenylglycinol was measured. Increased hydrogen ion concentration produced an increase in the observed fluorescence intensity change. This tendency of change is very similar to the retention factor change when using chiral crown ether as liquid chromatographic stationary phases,[17] indicating that the large enantioselectivity factors of amino alcohols are presumably because of the ability of the preferred enantiomers to “fill” the chiral cavity available to them on complexation with the crown ether entities in CCOF **17**. The formation of amino alcohol-crown ether adducts may affect proton-transfer-assisted charge-transfer excited state, leading to the fluorescence intensity changes.

To microscopically elucidate the interactions between (*R*)-CCOF **17** and D-/L-protonated PGL and reveal the chiral sensing mechanism, density functional theory (DFT) calculations were performed. First, potential energy surface scan was

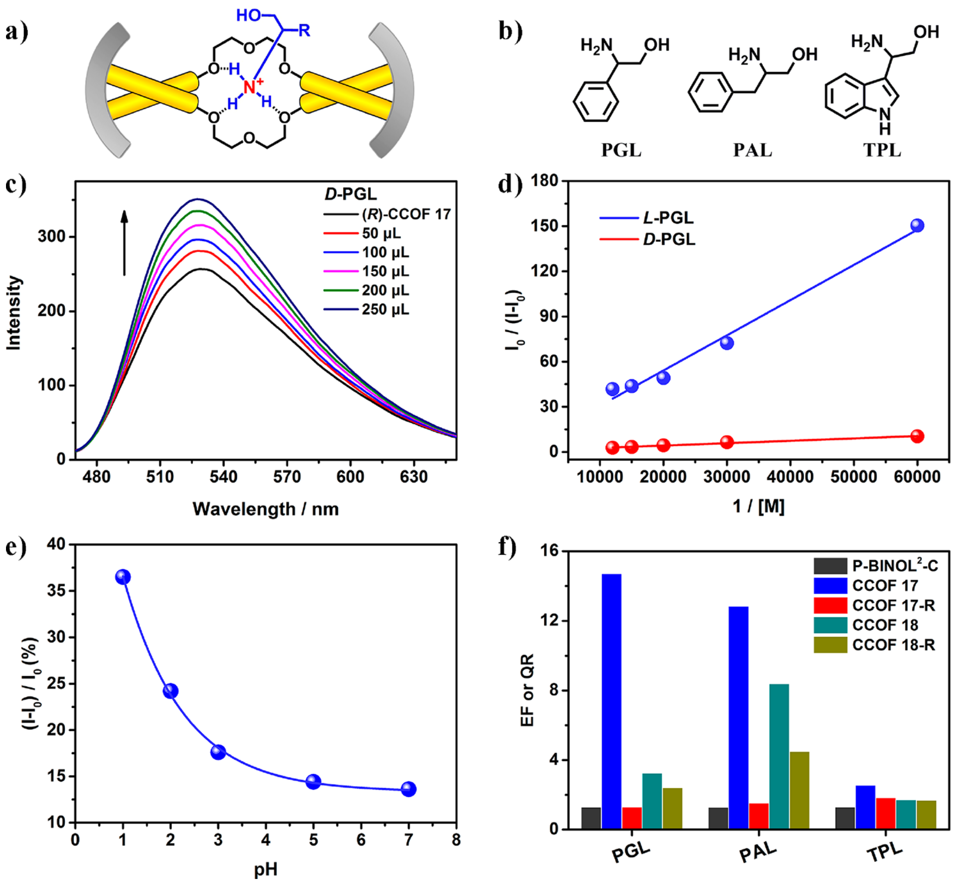

Figure 7. (a) Operation principle of the CCOF sensor. (b) Structures of the examined amino alcohols. (c) Fluorescence emission spectra of (*R*)-**17** with increasing concentration of D-phenylglycinol in solution. (d) Benesi−Hildebrand plots of the fluorescence emissions of (*R*)-**17** enhanced by D- and L-phenylglycinol. (e) The effect of pH values of $HClO_4$ aqueous solutions on fluorescence intensity. (f) The comparative EFs/QRs of the (*R*)-**P-BINOL²-C** and (*R*)-CCOFs for three amino alcohols.

conducted to identify the most stable conformations of isolated D-/L-protonated PGL (Figures S22 and S23), which were then used to explore the host−guest interactions. Various initial binding structures were examined for both enantiomers (Figure S24) over a two-layer ONIOM cluster model representing (*R*)-CCOF **17** (Figure S25). Figure 8 depicts the simplified structures of the most stable conformers of D-/L-protonated PGL with (*R*)-CCOF **17** (denoted as D-complex and L-complex, respectively). The corresponding complete structures with adjacent 2D COF layers can be found in Figures S26 and S27. In the D-complex, D-protonated PGL interacts with the crown ether group in (*R*)-CCOF **17** through three hydrogen bonds with H···O distances of 1.93, 2.46, and 2.72 Å and NH···O angles of 152°, 149°, and 136°, respectively. In the L-complex, L-protonated PGL coordinates with the crown ether group through three hydrogen bonds with H···O distances of 1.79, 2.49, and 2.27 Å and NH···O angles of 167°, 114°, and 144°, respectively. The phenyl group in D-/L-protonated PGL points away/toward the confined space constituted by adjacent 2D COF layers (Figures S26 and S27). At room temperature (298.15 K) and with methanol as a solvent, the relative Gibbs energy for L-complex is estimated to be 4.4 kcal/mol with respect to D-complex, indicating a preferential binding and sensing of D-enantiomer by (*R*)-CCOF **17**, which mainly results from more favorable host−guest coordination through hydrogen bonds and less steric hindrance imposed by the surrounding framework in D-complex as compared to that for the L-complex. These theoretical results well support the experimental observations (Figure 7).

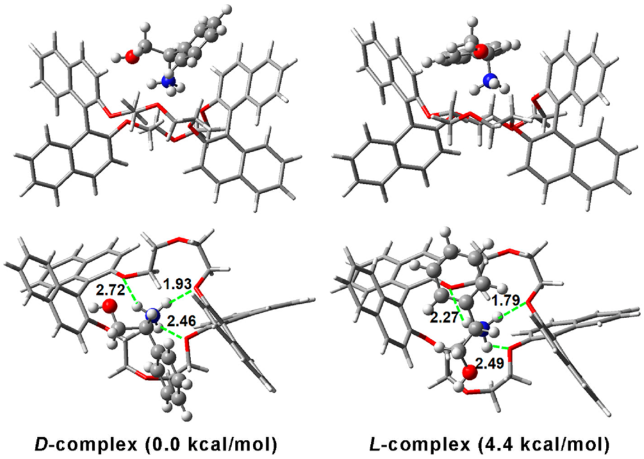

Figure 8. Side (upper) and top (lower) views of the lowest-energy structures of D-/L-protonated PGL with (*R*)-CCOF **17** (denoted as D-complex and L-complex, respectively). The relative Gibbs energies in methanol with respect to D-complex at 298.15 K are indicated in parentheses. The lengths (in Å) of hydrogen bonds involved in the host−guest interactions are labeled. The adjacent layers surrounding the host−guest complexes are omitted for clarity. C: gray, H: white, O: red, and N: blue.

The homogeneous control **P-BINOL^2-C** showed obvious fluorescence quenching toward all three amino alcohols, quite different from the observed for CCOF **17**. The QR values ranging from 1.28 to 1.30 were much smaller than the QR/EF values (4.72, 12.85, and 2.41) of CCOF **17**. This CCOF material is thus much sensitive than its molecular analog. Such a difference indicates that the porous CCOF is capable of providing a well-defined chiral environment for high enantiodiscrimination of amino alcohol enantiomer in comparison with **P-BINOL^2-C**. It should be noted that CCOF **17** show higher or comparable stereoselectivity to those reported BINOL-based sensors including organic molecules, organic oligomers, polymers, and coordination assemblies (Table S2).[18]

The change of fluorescence intensity of the CCOF is probably caused by static enhancement via the formation of a crown ether-amino alcohol adduct, which can affect the proton-transfer-assisted charge-transfer excited state.[19] For phenylglycinol and phenylalaninol, the formation of host−guest adducts between protonated amines and the immobilized crown ethers may lead to an increase in the interlayer space of COFs and weaken the $\pi-\pi$ interactions between CCOF layers, thereby causing the fluorescence intensity enhancement.[14] In contrast, besides binding the crown ethers, tryptophanol can establish $\pi-\pi$ interactions with the COF layers via the indole rings, as well as hydrogen interactions with crown ethers via the indole NH groups. Such newly formed $\pi-\pi$ stacking interactions may play a dominant role in influencing the COF fluorescence, causing decrease in the fluorescence intensity.[20] Further study is needed to understand the mechanism of the selective fluorescence changes. The static nature of the complexation is suggested by the consistent fluorescence lifetimes of the CCOF **17** suspensions before and after titration with D-phenylglycinol and D-tryptophanol (lifetime, τ_0, 1.15 vs 1.09 ns and 1.15 vs 1.53 ns, respectively). As the noncovalent interactions of the CCOFs with the enantiomers of amino alcohol afford different diastereomeric complexes, distinct fluorescence intensity change is thus detected.

As shown in Figure 7f, under otherwise identical conditions, CCOF **18** can also detect the three amino alcohols, with lower EF or QR to phenylglycinol, ohenylalaninol, and tryptophanol (3.26, 8.39, and 1.72, respectively) than CCOF **17**. In contrast, the reduced CCOFs showed low fluorescence change and selectivity toward the amino alcohols, with the EF/QR of 1.30, 1.53, and 1.84 for CCOF **17**-R and 2.41, 4.50, and 1.69 for CCOF **18**-R, respectively. It is clear that, for a given analyte, the enantioselectivity efficiency of C−C bond linked CCOF was lower than the C═C bond linked CCOF. This is probably caused by the destruction of the π-conjugate system after reduction, which may reduce the transmission and expression of chiral information in the 2D CCOF systems.[21] In addition, PXRD indicated that all CCOFs remained crystalline after treatment with D-phenylglycinol, indicative of the good stability of the frameworks (Figure S21).

■ CONCLUSION

We have demonstrated direct synthesis of the first two olefin-based CCOFs by Knoevenagel condensation of linear diacetonitriles and chiral tetraaldehyde derived from dibinaphthyl-22-crown-6. After postsynthetic reduction of the olefin linkages, the CCOFs were transformed into two isostructural C−C bond-linked frameworks. The complete reduction of C═C bonds was proved by FT-IR and ^{13}C NMR. All four CCOFs adopt a 2D layered tetragonal structure with slipped AA stacking and possess high crystallinity and porosity as well as high chemical stability in strong acids and bases. The newly formed C−C bond linkages leads to blue-shifted emissions of the parent structures with enhanced quantum yields and fluorescence lifetimes, and the olefin linked CCOFs show higher enantioseletivity than their reduced structures when they were utilized as fluorescence sensors for chiral amino alcohols. To the best of our knowledge, the present reduced frameworks are the first two examples of C−C bond-linked COFs and the unreduced frameworks are the first two examples of C═C bond-linked CCOFs. This work will promote the design and synthesis of more chemical stable COFs with strong linkages and new functions based on the solid-state conversions.

■ ASSOCIATED CONTENT

Supporting Information

The Supporting Information is available free of charge at https://pubs.acs.org/doi/10.1021/jacs.0c11050.

Detailed synthetic procedures, FT-IR spectra, TGA traces, TEM images, CD spectra, modeling details, dye uptake experiment, fluorescence data, DFT calculations, and gas adsorption (PDF)

Crystal structure data of CCOF **17** (CIF)

Crystal structure data of CCOF **17**-R (CIF)

Crystal structure data of CCOF **18** (CIF)

Crystal structure data of CCOF **18**-R (CIF)

■ AUTHOR INFORMATION

Corresponding Authors

Yan Liu − *School of Chemistry and Chemical Engineering, Frontiers Science Center for Transformative Molecules and State Key Laboratory of Metal Matrix Composites, Shanghai Jiao Tong University, Shanghai 200240, P. R. China;* orcid.org/0000-0002-7560-519X; Email: liuy@sjtu.edu.cn

Yong Cui − *School of Chemistry and Chemical Engineering, Frontiers Science Center for Transformative Molecules and State Key Laboratory of Metal Matrix Composites, Shanghai Jiao Tong University, Shanghai 200240, P. R. China;* orcid.org/0000-0003-1977-0470; Email: yongcui@sjtu.edu.cn

Authors

Chen Yuan − *School of Chemistry and Chemical Engineering, Frontiers Science Center for Transformative Molecules and State Key Laboratory of Metal Matrix Composites, Shanghai Jiao Tong University, Shanghai 200240, P. R. China;* orcid.org/0000-0003-0334-2594

Shiguo Fu − *School of Chemistry and Chemical Engineering, Frontiers Science Center for Transformative Molecules and State Key Laboratory of Metal Matrix Composites, Shanghai Jiao Tong University, Shanghai 200240, P. R. China*

Kuiwei Yang − *Department of Chemical and Biomolecular Engineering, National University of Singapore, Singapore 117585, Singapore*

Bang Hou − *School of Chemistry and Chemical Engineering, Frontiers Science Center for Transformative Molecules and State Key Laboratory of Metal Matrix Composites, Shanghai Jiao Tong University, Shanghai 200240, P. R. China;* orcid.org/0000-0002-3803-9520

Jianwen Jiang − *Department of Chemical and Biomolecular Engineering, National University of Singapore, Singapore 117585, Singapore;* orcid.org/0000-0003-1310-9024

Complete contact information is available at:
https://pubs.acs.org/10.1021/jacs.0c11050

Notes

The authors declare no competing financial interest.

■ ACKNOWLEDGMENTS

This work was financially supported by the National Science Foundation of China (Grant Nos. 21620102001, 91856204, 91956124, and 21875136), the National Key Basic Research Program of China (2016YFA0203400), Key Project of Basic Research of Shanghai (18JC1413200 and 19JC1412600), Shanghai Rising-Star Program (19QA1404300), and the Ministry of Education of Singapore and the National University of Singapore (C-261-000-207-532/C-261-000-777-532 and R-279-000-574-114).

■ REFERENCES

(1) (a) Côté, A. P.; Benin, A. I.; Ockwig, N. W.; O'Keeffe, M.; Matzger, A. J.; Yaghi, O. M. Porous, Crystalline, Covalent Organic Frameworks. *Science* **2005**, *310*, 1166−1170. (b) Ding, S. Y.; Wang, W. Covalent organic frameworks (COFs): from design to applications. *Chem. Soc. Rev.* **2013**, *42*, 548−568. (c) Ma, T.; Kapustin, E. A.; Yin, S. X.; Liang, L.; Zhou, Z.; Niu, J.; Li, L. H.; Wang, Y.; Su, J.; Li, J.; Wang, X.; Wang, W. D.; Wang, W.; Sun, J.; Yaghi, O. M. Single-crystal X-ray diffraction structures of covalent organic frameworks. *Science* **2018**, *361*, 48−52. (d) Evans, A. M.; Parent, L. R.; Flanders, N. C.; Bisbey, R. P.; Vitaku, E.; Kirschner, M. S.; Schaller, R. D.; Chen, L. X.; Gianneschi, N. C.; Dichtel, W. R. Seeded growth of single-crystal two-dimensional covalent organic frameworks. *Science* **2018**, *361*, 52−57. (e) Dong, J.; Han, X.; Liu, Y.; Li, H.; Cui, Y. Metal-covalent organic frameworks (MCOFs): A bridge between metal-organic frameworks and covalent organic frameworks. *Angew. Chem., Int. Ed.* **2020**, *59*, 13722−13733.

(2) (a) Furukawa, H.; Yaghi, O. M. Storage of hydrogen, methane, and carbon dioxide in highly porous covalent organic frameworks for clean energy applications. *J. Am. Chem. Soc.* **2009**, *131*, 8875−8883. (b) DeBlase, C. R.; Silberstein, K. E.; Truong, T.-T.; Abruna, H. D.; Dichtel, W. R. β-Ketoenamine-Linked Covalent Organic Frameworks Capable of Pseudocapacitive Energy Storage. *J. Am. Chem. Soc.* **2013**, *135*, 16821−16824. (c) Xu, F.; Xu, H.; Chen, X.; Wu, D.; Wu, Y.; Liu, H.; Gu, C.; Fu, R.; Jiang, D. Radical Covalent Organic Frameworks: A General Strategy to Immobilize Open-Accessible Polyradicals for High-Performance Capacitive Energy Storage. *Angew. Chem., Int. Ed.* **2015**, *54*, 6814−6818. (d) Lv, J. Q.; Tan, Y. X.; Xie, J. F.; Yang, R.; Yu, M. X.; Sun, S. S.; Li, M. D.; Yuan, D. Q.; Wang, Y. B. Direct Solar-to-Electrochemical Energy Storage in a Functionalized Covalent Organic Framework. *Angew. Chem., Int. Ed.* **2018**, *57*, 12716−12720.

(3) (a) Fu, J.; Das, S.; Xing, G.; Ben, T.; Valtchev, V.; Qiu, S. Fabrication of COF-MOF Composite Membranes and Their Highly Selective Separation of H_2/CO_2. *J. Am. Chem. Soc.* **2016**, *138*, 7673−7680. (b) Qian, H. L.; Yang, C. X.; Yan, X. P. Bottom-up synthesis of chiral covalent organic frameworks and their bound capillaries for chiral separation. *Nat. Commun.* **2016**, *7*, 12104. (c) Fan, H.; Gu, J.; Meng, H.; Knebel, A.; Caro, J. High-Flux Membranes Based on the Covalent Organic Framework COF-LZU1 for Selective Dye Separation by Nanofiltration. *Angew. Chem., Int. Ed.* **2018**, *57*, 4083−4087. (d) Huang, J.; Han, X.; Yang, S.; Cao, Y.; Yuan, C.; Liu, Y.; Wang, J.; Cui, Y. Microporous 3D Covalent Organic Frameworks for Liquid Chromatographic Separation of Xylene Isomers and Ethylbenzene. *J. Am. Chem. Soc.* **2019**, *141*, 8996−9003.

(4) (a) Lu, S.; Hu, Y.; Wan, S.; McCaffrey, R.; Jin, Y.; Gu, H.; Zhang, W. Synthesis of Ultrafine and Highly Dispersed Metal Nanoparticles Confined in a Thioether-Containing Covalent Organic Framework and Their Catalytic Applications. *J. Am. Chem. Soc.* **2017**, *139*, 17082−17088. (b) Pachfule, P.; Acharjya, A.; Roeser, J.; Langenhahn, T.; Schwarze, M.; Schomaecker, R.; Thomas, A.; Schmidt, J. Diacetylene Functionalized Covalent Organic Framework (COF) for Photocatalytic Hydrogen Generation. *J. Am. Chem. Soc.* **2018**, *140*, 1423−1427. (c) Bhadra, M.; Kandambeth, S.; Sahoo, M. K.; Addicoat, M.; Balaraman, E.; Banerjee, R. Triazine Functionalized Porous Covalent Organic Framework for Photo-organocatalytic *E*−*Z* Isomerization of Olefins. *J. Am. Chem. Soc.* **2019**, *141*, 6152−6156.

(5) (a) El-Kaderi, H. M.; Hunt, J. R.; Mendoza-Cortes, J. L.; Côté, A. P.; Taylor, R. E.; O'Keeffe, M.; Yaghi, O. M. Designed synthesis of 3D covalent organic frameworks. *Science* **2007**, *316*, 268−272. (b) Jakowetz, A. C.; Hinrichsen, T. F.; Ascherl, L.; Sick, T.; Calik, M.; Auras, F.; Medina, D. D.; Friend, R. H.; Rao, A.; Bein, T. Excited-State Dynamics in Fully Conjugated 2D Covalent Organic Frameworks. *J. Am. Chem. Soc.* **2019**, *141*, 11565−11571. (c) Uribe-Romo, F. J.; Doonan, C. J.; Furukawa, H.; Oisaki, K.; Yaghi, O. M. Crystalline Covalent Organic Frameworks with Hydrazone Linkages. *J. Am. Chem. Soc.* **2011**, *133*, 11478−11481. (d) Hao, L.; Ning, J.; Luo, B.; Wang, B.; Zhang, Y.; Tang, Z.; Yang, J.; Thomas, A.; Zhi, L. Structural Evolution of 2D Microporous Covalent Triazine-Based Framework toward the Study of High-Performance Supercapacitors. *J. Am. Chem. Soc.* **2015**, *137*, 219−225. (e) Meng, Z.; Stolz, R. M.; Mirica, K. A. Two-Dimensional Chemiresistive Covalent Organic Framework with High Intrinsic Conductivity. *J. Am. Chem. Soc.* **2019**, *141*, 11929−11937. (f) Wei, P.; Qi, M.; Wang, Z.; Ding, S.; Yu, W.; Liu, Q.; Wang, L.; Wang, H.; An, W.; Wang, W. Benzoxazole-Linked Ultrastable Covalent Organic Frameworks for Photocatalysis. *J. Am. Chem. Soc.* **2018**, *140*, 4623−631. (g) Guan, X.; Li, H.; Ma, Y.; Xue, M.; Fang, Q.; Yan, Y.; Valtchev, V.; Qiu, S. Chemically stable polyarylether-based covalent organic frameworks. *Nat. Chem.* **2019**, *11*, 587−594. (h) Zhang, B.; Wei, M. F.; Mao, H. Y.; Pei, X. K.; Alshmimri, S. A.; Reimer, J. A.; Yaghi, O. M. Crystalline Dioxin-Linked Covalent Organic Frameworks from Irreversible Reactions. *J. Am. Chem. Soc.* **2018**, *140*, 12715−12719. (i) Wei, S.; Zhang, F.; Zhang, W.; Qiang, P.; Yu, K.; Fu, X.; Wu, D.; Bi, S.; Zhang, F. Semiconducting 2D Triazine-Cored Covalent Organic Frameworks with Unsubstituted Olefin Linkages. *J. Am. Chem. Soc.* **2019**, *141*, 14272−14279. (j) Lyu, H.; Diercks, C. S.; Zhu, C.; Yaghi, O. M. Porous Crystalline Olefin-Linked Covalent Organic Frameworks. *J. Am. Chem. Soc.* **2019**, *141*, 6848−6852.

(6) (a) Van Humbeck, J. F.; McDonald, T. M.; Jing, X.; Wiers, B. M.; Zhu, G.; Long, J. R. Ammonia Capture in Porous Organic Polymers Densely Functionalized with Brønsted Acid Groups. *J. Am. Chem. Soc.* **2014**, *136*, 2432−2440. (b) Liu, W.; Luo, X.; Bao, Y.; Liu, Y. P.; Ning, G. H.; Abdelwahab, I.; Li, L.; Nai, C. T.; Hu, Z. G.; Zhao, D.; Liu, B.; Quek, S. Y.; Loh, K. P. A Two-Dimensional Conjugated Aromatic Polymer via C−C Coupling Reaction. *Nat. Chem.* **2017**, *9*, 563−570. (c) Zhou, D.; Tan, X. Y.; Wu, H. M.; Tian, L. H.; Li, M. Synthesis of C−C Bonded Two-Dimensional Conjugated Covalent Organic Framework Films by Suzuki Polymerization on a Liquid-Liquid Interface. *Angew. Chem., Int. Ed.* **2019**, *58*, 1376−1381.

(7) (a) Xu, H.; Gao, J.; Jiang, D. L. Stable, crystalline, porous, covalent organic frameworks as a platform for chiral organocatalysts. *Nat. Chem.* **2015**, *7*, 905−912. (b) Wang, X. R.; Han, X.; Zhang, J.; Wu, X. W.; Liu, Y.; Cui, Y. Homochiral 2D Porous Covalent Organic Frameworks for Heterogeneous Asymmetric Catalysis. *J. Am. Chem. Soc.* **2016**, *138*, 12332−12335. (c) Zhang, J.; Han, X.; Wu, X. W.; Liu, Y.; Cui, Y. Multivariate Chiral Covalent Organic Frameworks with Controlled Crystallinity and Stability for Asymmetric Catalysis. *J. Am. Chem. Soc.* **2017**, *139*, 8277−8285. (d) Han, X.; Xia, Q. C.; Huang, J. J.; Liu, Y.; Tan, C. X.; Cui, Y. Chiral Covalent Organic Frameworks with High Chemical Stability for Heterogeneous Asymmetric Catalysis. *J. Am. Chem. Soc.* **2017**, *139*, 8693−8697. (e) Sun, Q.; Fu, C. W.; Aguila, B.; Perman, J.; Wang, S.; Huang, H. Y.; Xiao, F. S.; Ma, S. Q. Pore Environment Control and Enhanced Performance of Enzymes Infiltrated in Covalent Organic Frameworks. *J. Am. Chem. Soc.* **2018**, *140*, 984−992. (f) Han, X.; Huang, J. J.; Yuan, C.; Liu, Y.;

Cui, Y. Chiral 3D Covalent Organic Frameworks for High Performance Liquid Chromatographic Enantioseparation. *J. Am. Chem. Soc.* **2018**, *140*, 892−895. (g) Barragan-Iglesias, P.; Lou, T.-F.; Bhat, V. D.; Megat, S.; Burton, M. D.; Price, T. J.; Campbell, Z. T. Chiral induction in covalent organic frameworks. *Nat. Commun.* **2018**, *9*, 10. (h) Wu, X. W.; Han, X.; Xu, Q. S.; Liu, Y. H.; Yuan, C.; Yang, S.; Liu, Y.; Jiang, J. W.; Cui, Y. Chiral BINOL-Based Covalent Organic Frameworks for Enantioselective Sensing. *J. Am. Chem. Soc.* **2019**, *141*, 7081−7089. (i) Yuan, C.; Wu, X. W.; Gao, R.; Han, X.; Liu, Y.; Long, Y. T.; Cui, Y. Nanochannels of Covalent Organic Frameworks for Chiral Selective Transmembrane Transport of Amino Acids. *J. Am. Chem. Soc.* **2019**, *141*, 20187−20197. (j) Wang, L. K.; Zhou, J. J.; Lan, Y. B.; Ding, S. Y.; Yu, W.; Wang, W. Divergent Synthesis of Chiral Covalent Organic Frameworks. *Angew. Chem., Int. Ed.* **2019**, *58*, 9443−9447. (k) Ma, H. C.; Zhao, C. C.; Chen, G. J.; Dong, Y. B. Photothermal Conversion Triggered Thermal Asymmetric Catalysis within Metal Nanoparticles Loaded Homochiral Covalent Organic Framework. *Nat. Commun.* **2019**, *10*, 3368. (l) Ma, H. C.; Chen, G. J.; Huang, F.; Dong, Y. B. Homochiral Covalent Organic Framework for Catalytic Asymmetric Synthesis of a Drug Intermediate. *J. Am. Chem. Soc.* **2020**, *142*, 12574−12578. (m) Xu, H. S.; Ding, S. Y.; An, W. K.; Wu, H.; Wang, W. Constructing Crystalline Covalent Organic Frameworks from Chiral Building Blocks. *J. Am. Chem. Soc.* **2016**, *138*, 11489−11492.

(8) Han, X.; Yuan, C.; Hou, B.; Liu, L.; Li, H.; Liu, Y.; Cui, Y. Chiral covalent organic frameworks: design, synthesis and property. *Chem. Soc. Rev.* **2020**, *49*, 6248−6272.

(9) (a) Waller, P. J.; Lyle, S. J.; Osborn Popp, T. M.; Diercks, C. S.; Reimer, J. A.; Yaghi, O. M. Chemical Conversion of Linkages in Covalent Organic Frameworks. *J. Am. Chem. Soc.* **2016**, *138*, 15519−15522. (b) Liu, H. Y.; Chu, J.; Yin, Z. L.; Cai, X.; Zhuang, L.; Deng, H. X. Covalent Organic Frameworks Linked by Amine Bonding for Concerted Electrochemical Reduction of CO_2. *Chem.* **2018**, *4*, 1696−1709. (c) Waller, P. J.; Al Faraj, Y. S.; Diercks, C. S.; Jarenwattananon, N. N.; Yaghi, O. M. Conversion of Imine to Oxazole and Thiazole Linkages in Covalent Organic Frameworks. *J. Am. Chem. Soc.* **2018**, *140*, 9099−9103. (d) Li, X.; Zhang, C.; Cai, S.; Lei, X.; Altoe, V.; Hong, F.; Urban, J. J.; Ciston, J.; Chan, E. M.; Liu, Y. Facile Transformation of Imine Covalent Organic Frameworks into Ultrastable Crystalline Porous Aromatic Frameworks. *Nat. Commun.* **2018**, *9*, 2998.

(10) (a) Zhang, X. X.; Bradshaw, J. S.; Izatt, R. M. Enantiomeric recognition of amine compounds by chiral macrocyclic receptors. *Chem. Rev.* **1997**, *97*, 3313−3361. (b) Gokel, G. W.; Leevy, W. M.; Weber, M. E. Crown ethers: Sensors for ions and molecular scaffolds for materials and biological models. *Chem. Rev.* **2004**, *104*, 2723−2750.

(11) (a) Ngo, H. L.; Lin, W. Chiral Crown Ether Pillared Lamellar Lanthanide Phosphonates. *J. Am. Chem. Soc.* **2002**, *124*, 14298−14299. (b) Zhao, Y. L.; Liu, L. H.; Zhang, W. Y.; Sue, C. H.; Li, Q. W.; Miljanic, O. S.; Yaghi, O. M.; Stoddart, J. F. Rigid-Strut-Containing Crown Ethers and [2] Catenanes for Incorporation into Metal-Organic Frameworks. *Chem. - Eur. J.* **2009**, *15*, 13356−13380. (c) Valente, C.; Choi, E.; Belowich, M. E.; Doonan, C. J.; Li, Q. W.; Gasa, T. B.; Botros, Y. Y.; Yaghi, O. M.; Stoddart, J. F. Metal-organic frameworks with designed chiral recognition sites. *Chem. Commun.* **2010**, *46*, 4911−4913.

(12) (a) Pu, L. Enantioselective Fluorescent Sensors: A Tale of BINOL. *Acc. Chem. Res.* **2012**, *45*, 150−163. (b) Parmar, D.; Sugiono, E.; Raja, S.; Rueping, M. Complete Field Guide to Asymmetric BINOL-Phosphate Derived Bronsted Acid and Metal Catalysis: History and Classification by Mode of Activation; Bronsted Acidity, Hydrogen Bonding, Ion Pairing, and Metal Phosphates. *Chem. Rev.* **2014**, *114*, 9047−9153.

(13) (a) Kang, X.; Han, X.; Yuan, C.; Cheng, C.; Liu, Y.; Cui, Y. Reticular Synthesis of tbo Topology Covalent Organic Frameworks. *J. Am. Chem. Soc.* **2020**, *142*, 16346−16356. (b) Shin, S. M.; Lee, M. S.; Han, J. H.; Jeong, N. Assessing the guest-accessible volume in MOFs using two-photon fluorescence microscopy. *Chem. Commun.* **2014**, *50*, 289−291.

(14) (a) Dalapati, S.; Jin, E.; Addicoat, M.; Heine, T.; Jiang, D. Highly Emissive Covalent Organic Frameworks. *J. Am. Chem. Soc.* **2016**, *138*, 5797−5800. (b) Zhu, M. W.; Xu, S. Q.; Wang, X. Z.; Chen, Y. Q.; Dai, L. Y.; Zhao, X. The construction of fluorescent heteropore covalent organic frameworks and their applications in spectroscopic and visual detection of trinitrophenol with high selectivity and sensitivity. *Chem. Commun.* **2018**, *54*, 2308−2311. (c) Gao, Q.; Li, X.; Ning, G. H.; Leng, K.; Tian, B. B.; Liu, C. B.; Tang, W.; Xu, H. S.; Loh, K. P. Highly photoluminescent two-dimensional imine-based covalent organic frameworks for chemical sensing. *Chem. Commun.* **2018**, *54*, 2349−2352.

(15) (a) Pu, L. Fluorescence of organic molecules in chiral recognition. *Chem. Rev.* **2004**, *104*, 1687−1716. (b) You, L.; Zha, D. J.; Anslyn, E. V. Recent Advances in Supramolecular Analytical Chemistry Using Optical Sensing. *Chem. Rev.* **2015**, *115*, 7840−7892.

(16) (a) Kyba, E. B.; Koga, K.; Sousa, L. R.; Siegel, M. G.; Cram, D. J. Chiral Recognition in Molecular Complexing. *J. Am. Chem. Soc.* **1973**, *95*, 2692. (b) Li, J.; Yim, D.; Jang, W. D.; Yoon, J. Recent progress in the design and applications of fluorescence probes containing crown ethers. *Chem. Soc. Rev.* **2017**, *46*, 2437−2458.

(17) Udvarhelyi, P. M.; Watkins, J. C. Direct resolution of some phenylglycines by liquid chromatography on a chiral crown ether phase. *Chirality* **1990**, *2*, 200−204.

(18) (a) Wang, Q.; Chen, X.; Tao, L.; Wang, L.; Xiao, D.; Yu, X. Q.; Pu, L. Enantioselective fluorescent recognition of amino alcohols by a chiral tetrahydroxyl 1,1′-binaphthyl compound. *J. Org. Chem.* **2007**, *72*, 97−101. (b) Cho, E. N. R.; Li, Y.; Kim, H. J.; Hyun, M. H. A Colorimetric Chiral Sensor Based on Chiral Crown Ether for the Recognition of the Two Enantiomers of Primary Amino Alcohols and Amines. *Chirality* **2011**, *23*, 349−353. (c) Wanderley, M. M.; Wang, C.; Wu, C. D.; Lin, W. B. A Chiral Porous Metal-Organic Framework for Highly Sensitive and Enantioselective Fluorescence Sensing of Amino Alcohols. *J. Am. Chem. Soc.* **2012**, *134*, 9050−9053. (d) Wei, J.; Zhang, X. M.; Zhao, Y. P.; Li, R. X. Chiral Conjugated Microporous Polymers as Novel Chiral Fluorescence Sensors for Amino Alcohols. *Macromol. Chem. Phys.* **2013**, *214*, 2232−2238. (e) Jiao, J. M.; Wei, G.; Li, F.; Mao, X. R.; Cheng, Y. X.; Zhu, C. J. (*S*)-BINOL-based boronic ester fluorescence sensors for enantioselective recognition of α-phenylethylamine and phenylglycinol. *RSC Adv.* **2014**, *4*, 5887−5892. (f) Zhang, X. P.; Wang, C.; Wang, P.; Du, J. J.; Zhang, G. Q.; Pu, L. Conjugated polymer-enhanced enantioselectivity in fluorescent sensing. *Chem. Sci.* **2016**, *7*, 3614−3620. (g) Wang, C.; Anbaei, P.; Pu, L. Highly Enantioselective Fluorescent Recognition of Both Unfunctionalized and Functionalized Chiral Amines by a Facile Amide Formation from a Perfluoroalkyl Ketone. *Chem. - Eur. J.* **2016**, *22*, 7255−7261. (h) Muralidharan, V. P.; Sathiyanarayanan, K. I. Naphthalimide-Based Chiral Fluorescence Sensor Employing (*S*)-BINOL Unit for Highly Enantioselective Recognition of α-Amino Alcohols with Opposite Chiral Selectivity. *ChemistrySelect* **2018**, *3*, 3111−3117. (i) Tan, C. X.; Yang, K. W.; Dong, J. Q.; Liu, Y. H.; Liu, Y.; Jiang, J. W.; Cui, Y. Boosting Enantioselectivity of Chiral Organocatalysts with Ultrathin Two-Dimensional Metal-Organic Framework Nanosheets. *J. Am. Chem. Soc.* **2019**, *141*, 17685−17695.

(19) (a) Shizuka, H. Excited-State Proton-Transfer Reactions and Proton-Induced Quenching of Aromatic Compounds. *Acc. Chem. Res.* **1985**, *18*, 141−147. (b) Zhou, P.; Han, K. Unraveling the Detailed Mechanism of Excited-State Proton Transfer. *Acc. Chem. Res.* **2018**, *51*, 1681−1690.

(20) (a) Albacete, P.; Martínez, J. I.; Li, X.; López-Moreno, A.; Mena-Hernando, S. A.; Platero-Prats, A. E.; Montoro, C.; Loh, K. P.; Pérez, E. M.; Zamora, F. Layer-stacking-driven fluorescence in a two-dimensional imine-linked covalent organic framework. *J. Am. Chem. Soc.* **2018**, *140*, 12922−12929. (b) Haug, W. K.; Moscarello, E. M.; Wolfson, E. R.; McGrier, P. L. The luminescent and photophysical properties of covalent organic frameworks. *Chem. Soc. Rev.* **2020**, *49*, 839−864.

(21) (a) Lv, W.; Zhu, P.; Bian, Y.; Ma, C.; Zhang, X.; Jiang, J. Optically Active Homoleptic Bis(phthalocyaninato) Rare Earth Double-Decker Complexes Bearing Peripheral Chiral Menthol Moieties: Effect of π−π Interaction on the Chiral Information Transfer at the Molecular Level. *Inorg. Chem.* **2010**, *49*, 6628−6635. (b) Yang, Y.; Zhang, Y.; Wei, Z. Supramolecular Helices: Chirality Transfer from Conjugated Molecules to Structures. *Adv. Mater.* **2013**, *25*, 6039−6049.

https://dx.doi.org/10.1021/jacs.0c11050
J. Am. Chem. Soc. XXXX, XXX, XXX−XXX